Impact of Aerosols and Atmospheric Thermodynamics on Cloud Properties within the Climate System

Toshihisa Matsui, Hirohiko Masunaga, Roger Pielke Sr.
and Wei-Kuo Tao

Submitted to ***Geographic Research Letter***

Popular Summary

A combination of cloud-top and columnar droplet sizes derived from the multi Tropical Rainfall Measurement Mission (TRMM) sensors reveals the sensitivity of the aerosols effect on cloud-precipitation process due to environmental vertical thermodynamic structure. First, the magnitude of aerosol indirect effect could be larger with the analysis of columnar droplet sizes than that derived from the cloud-top droplet sizes, since column-droplet size can account for the broader droplet spectra in the cloud layers. Second, a combination of cloud-top and columnar droplet sizes reveals that the warm rain process is prevented regardless of the aerosols concentration under a high static stability such as when a strong temperature inversion exists, while a high aerosol concentration suppresses the warm rain formulation under a low static stability.

Impact of Aerosols and Atmospheric Thermodynamics on Cloud Properties within the Climate System

Toshihisa Matsui, Hirohiko Masunaga and Roger Pielke Sr.
Department of Atmospheric Science
Colorado State University
Ft. Collins, CO 80523-1371

Wei-Kuo Tao
Laboratory for Atmospheres
NASA Goddard Space Flight Center
Greenbelt, MD 20771

Submitted on Dec 12, 2003

[1] **Abstract.** A combination of cloud-top and columnar droplet sizes derived from the multi Tropical Rainfall Measurement Mission (TRMM) sensors reveals the sensitivity of the aerosols effect on cloud-precipitation process due to environmental vertical thermodynamic structure. First, the magnitude of aerosol indirect effect could be larger with the analysis of columnar droplet sizes than that derived from the cloud-top droplet sizes, since column-droplet size can account for the broader droplet spectra in the cloud layers. Second, a combination of cloud-top and columnar droplet sizes reveals that the warm rain process is prevented regardless of the aerosols concentration under a high static stability such as when a strong temperature inversion exists, while a high aerosol concentration suppresses the warm rain formulation under a low static stability.

1. Introduction

[2] Maritime low clouds play a key role in the earth's energy budget through an imbalance between the long wave emission and the reflection of solar radiation. Observations indicate that extensive low clouds, denoted hereafter as stratus, reduce the earth's net radiation by approximately 15 (W/m_) in an annual average [*Hartmann et al.,* 1992]. This large sensitivity of stratus to the earth's radiation budget has motivated studies to examine the factors governing the microphysical properties of stratus.

[3] Stratus amount is, in particular, positively correlated with lower-tropospheric static

stability (LTSS), defined as the potential temperature difference between a surface and the 700 (mb) pressure level [*Klein and Hartmann,* 1993]. High LTSS represents a strong temperature inversion at the top of the atmospheric boundary layer, which prevents clouds from developing into deep cumulus convection. High LTSS is frequently observed over the subtropical region and off coasts where warm continental air flows over cold sea surface temperatures (SSTs). In these regions, clouds are confined to the boundary layer, constraining the cloud droplet growth and liquid water path (LWP), while extending their horizontal areal coverage and lifetime.

[4] Another important factor that controls the stratus properties are *aerosols,* as they acting as cloud condensation nuclei (CCN) to form cloud droplets. In a polluted region, a high concentration of the aerosols over-seeds cloud droplets to generate highly concentrated, narrowly distributed cloud droplet spectra, which results in a larger surface area that increases the reflection of solar radiation up to 30 % [*Twomey,* 1984]. Narrowly distributed cloud droplet spectra prevent a formulation of precipitation, and could increase the cloud lifetime and horizontal areal coverage that further cool earth's surface [*Albrecht,* 1989]. This climatic impact of the aerosols on the cloud properties, denoted as the aerosol indirect effect, is yet one of the largest uncertainties in accurately describing the earth's radiation budget and the sensitivity of the climate to changes in aerosol concentrations in the future.

[5] Figure 1 exhibits a global distribution of seasonally averaged LTSS (color contours) derived from the NCEP/NCAR reanalysis [*Kalnay et al.,* 1996] and seasonally averaged aerosol index derived from the MODerate resolution Imaging Spectroradiometer (MODIS) (dark shaded) [*Tanré et al.,* 1997]. Aerosol index is better correlated with the column aerosol concentrations under some assumptions [*Nakajima et al.,* 2001; *Bréon et al.,* 2002], and was derived from a product of the aerosol optical thickness at 0.55 (μm) and Ångstrom exponent computed from 0.55 and 0.865 (μm). Generally, the global atmospheric circulation determines the distribution of LTSS, whereas the regional distribution and magnitude of aerosol sources, and the seasonal meteorological patterns determine the concentrations of aerosols over the ocean and the land [*Kaufman et al.,* 2002]. Different contributions from these two factors across the globe possibly influence the cloud microstructure. This paper examines the sensitivity of the aerosol effect on global clouds properties due to the background atmospheric thermodynamic structure.

2. TRMM-derived cloud properties

[6] A new algorithm using the Tropical Rainfall Measurement Mission (TRMM) Microwave Imager (TMI) and Visible/Infrared Radiance Imager (VIRS) provides the vertical structure of warm cloud (cloud top temperature > 273 K) microstructure via investigating two types of droplet effective radius (Re): shortwave-derived droplet size (Re (top)) and microwave-derived droplet size (Re (column)). This is because, a VIRS-derived Re tends to be biased toward a cloud-top value due to strong absorption of the near-infrared band, whereas a TMI-derived Re is expected to be close to the value averaged over the cloud layer since microwave does not suffer from saturation within low maritime clouds [*Masunaga et al.,* 2002a].

[7] A scatter plot (Figure 2.a) shows the relationship between seasonally (March – May) averaged Re (top) and Re (column) at each grid in the global tropics. Re (top) generally ranges from 10 to 21 (μm), whereas Re (column) broadly ranges up to 50 (μm). A large blurring of Re (column) exists at Re (top) > 15 (μm) because of the error and natural variability associated with daytime cloud diurnal cycles observed from the TRMM satellite. Figure 2.a can be used to judge different cloud modes [*Masunaga et al.,* 2002b]. In this study, we used Re (column) in the y-axis and add the solid line to represent the unity ratio between Re (top) and Re (column).

[8] When Re (top) are less than the critical threshold of drizzling at 15 (μm), Re (column) tends to be concentrated beneath the solid line, which represents that Re (column) are generally smaller than Re (top) at Re (top) < 15 (μm); i.e., cloud droplet sizes increase toward the cloud top. Thus, clouds in the zone-I represent no precipitation of any type in this cloud, and are assigned as *non-precipitating*. When Re (top) exceeds at 15 (μm), Re (column) begins to increase dramatically. Clouds with Re (top) > 15 (μm) and Re (column) < 15 (μm) suggest the presence of drizzling at the cloud top; however the droplets still increase in size toward the cloud top. They are unlikely to produce considerable amounts of precipitation. Thus, clouds in this zone-II are assigned as *transitional.* Cloud with Re (top) > 15 (μm) and Re (column) > 15 (μm), Re (column) is mostly likely to exceed the Re (top); i.e., droplet sizes increase toward the cloud base, indicating the presence of larger precipitation-size droplets near the cloud base. Thus, clouds in the zone-III are assigned as *precipitating.* In a small number of clouds, Re (column) is greater than the Re (top), although Re (top) does not exceeds the drizzle threshold. Clouds in zone-IV are assigned as *uncertain.*

[9] Since cloud properties generally transform gradually instead of at the given drizzle boundaries, a color coordination is assigned to represent the degree of the cloud mode (Figure

1.b), and it is applied for a global map of four cloud modes through overlaying the global distribution of Re (column) and Re (top) (Figure 2.a). Non-precipitating stratus (red) exist toward down-wind of continents, including off the coast of the Namibia, the Mediterranean Sea, the East China Sea, North America, South America, and the central Atlantic Ocean extended from West Africa. Those regions are generally characterized with polluted (a high aerosol index) and/or stable atmosphere (high LTSS) (Figure 1). The stratus in the rest of the subtropical region characterized with relatively polluted and moderately stable atmosphere is the transitional mode (green). It may be surprising that transitional stratus is found in the Inter Tropical Convergence Zone and the Pacific Warm Pool. In these regions, the precipitation process is dominated by deep cumulus convection (cold-rain process), which promotes a subsidence in the surrounding warm clouds [*Johnson et al.,* 1995].

[10] Precipitating stratus (blue) is found in the outer fringes of the tropical rain area, including the north and south pacific, the Indian Ocean and the Atlantic Ocean. Those regions is, compared regions with non-precipitating stratus, generally characterized with pristine (a low aerosols index) and/or less stable atmosphere (lower LTSS) (Figure 1). Uncertain stratus (black) is present in a small portion of the north Indian Ocean and Caribbean Sea. The sampling number of the uncertain stratus is very small (7.3% of total) compared with areas of the other cloud modes. This categorization is supported by *Masunaga et al.,* [2002b]. The distribution of the precipitating stratus is also associated with the areas where the warm rain process is observed by the TRMM Precipitation Radar [*Schumacher and Houze,* 2003].

3. Sensitivity of the Aerosol Indirect Effect

a. Method

[11] Although the possible relationship exists between the spatial distribution of cloud modes, aerosol index, and LTSS (Figure 1 & 3), it is difficult to quantify the relationship from the seasonal mean values. Thus, we performed a statistical analysis for the individual estimates of stratus, aerosol index and LTSS. The three individual datasets are not precisely concurrent in time and space.

[12] We directly relate the daily 1-degree MODIS aerosol index, 0.25-degree TRMM cloud properties and 2.5-degree LTSS from the NCEP/NCAR reanalysis without spatial interpolation. The maximum difference of overpass timing between the TRMM and the MODIS is set to be 3

hours, reducing the error associated with the different satellite overpass. The LTSS from the NCEP/NCAR reanalysis is linearly interpolated for the TRMM overpass timing. The total sampling number of the quasi-coincident observations was 462,289; 287,007 of the total were observed in the subtropical region (25°-37°N and 25°-37°S), while 170,304 of the total were observed in the tropics (25°S – 25°N).

b. Result

[13] The mean and standard error ($\sigma/\sqrt{n-2}$, where n and _ are the number of quasi-coincident measurements for each bin and is standard deviation, respectively) of Re (top) and Re (column) were derived with a given aerosol index (bins of 0.02) and LTSS (bins of 0.4 K) (Figure 4). The three-dimensional slope shows that high aerosol index and/or high LTSS leads to the smaller droplet size in both Re (column) and Re (top); i.e., a larger temperature inversion and higher concentrations of aerosols inhibit cloud droplet growth. On the other hand, cloud droplet sizes are maximized in the pristine (the lowest aerosol index) and less stable atmosphere (the lowest LTSS).

[14] For fixed liquid water path, the relationship between *Re* and aerosol index is expressed as [e.g., *Bréon et al.*, 2002]

$$\frac{d\log(\mathrm{Re})}{d\log(AI)} = \frac{\alpha}{3}, \qquad (1)$$

where AI is aerosol index, and α approximately relates the aerosol index to the number of cloud droplets (N_c) via $N_c \approx (AI)^{\alpha}$. The slope ($\alpha/3$) is a parameter that simply quantify the magnitude of aerosol indirect effect. Since the standard errors are generally larger for the bins of higher aerosol index due to a lack of the sample number (Figure 4), we derived the slope ($\alpha/3$) for an aerosol index > 0.25. The slope ($\alpha/3$) of Re (top) averaged over a full range of LTSS (Figure 4) is 0.069. Although our sampling and statistical processes are different from the previous studies in a strict manner, the value (0.069) is close to that derived from the Polarization and Directionality of the Earth Reflectance (POLDER) instrument (0.085) [*Bréon et al.*, 2002] and less than 50 % of that derived from the Advanced High Resolution Radiometer (AVHRR) (0.16) [*Nakajima et al.*, 2001]. On the other hand, the slope of Re (column) is 0.222, which is three times larger than that of Re (top), and is close to that using a characteristic value, $\alpha = 0.7$ [*Charlson et al.*, 1992]. Since the Re (column) is directly related to the cloud optical depth

[*Masunaga et al.*, 2002a], the aerosol indirect effect and associated earth's cooling effect could be greater than the estimation with using cloud-top Re (-0.7-0.2 W/m_) [*Nakajima et al.,* 2001].

[15] Figure 4.a also indicates that the slope ($\alpha/3$) varies in different LTSS. The slopes of Re (column) averaged over the five bins of LTSS range from 0.12 to 0.32 (Table 1). In the same LTSS intervals, the slope of Re (top) range from 0.022 to 0.071. Those contain values derived over land and ocean [*Bréon et al.,* 2002], suggesting that the difference in the slope between land and ocean could be explained by their background thermodynamic structure, in addition to observational tendency of the POLDER sensor [*Rosenfeld and Feingold,* 2003]. Except for the lowest LTSS intervals (12.2 – 13.8), the slope of Re (column) and Re (top) generally decreases toward the higher LTSS (Table 1); i.e., a greater fraction of aerosols are converted into cloud droplets in the lower LTSS with respect to the equation 2. This result is also physically reasonable, since a lower static stability permits a deeper atmospheric boundary layer and stronger updrafts to yield a higher supersaturation, which activate more CCNs thereby decreasing the droplet size [*Feingold et al.,* 2003]. However, the aerosol effect on the cloud albedo and associated earth's radiation budget is not necessarily stronger in the convectively unstable atmosphere, since cloud areal coverage becomes very small in such regions [*Klein and Hartmann,* 1993]. The different slopes (Figure 4) due to the LTSS also explains why the mean slope ($\alpha/3$) of Re (top) is smaller than that using the similar algorithm and remote sensor [*Nakajima et al.,* 2001]; our statistical sampling number is biased toward the subtropical regions, where the LTSS is, in general, higher than the tropical region. As a result, the slope ($\alpha/3$) of Re (top) becomes smaller in this study.

[16] Finally, a combination of mean Re (top) and Re (column) provide the distribution of the cloud modes as functions of the aerosol index and the LTSS with the color coordination in the Figure 2.b (Figure 5). Precipitating stratus (blue) exist when aerosol index and LTSS are less than approximately 0.08 and 16.8, respectively. Non-precipitating stratus (red) exists with a high aerosol index (~0.24). Transitional stratus (green) lies between the non-precipitating and precipitating stratus. The boundaries of three cloud modes are tilted toward the higher LTSS. The figure 5 clearly shows that a high aerosol concentration suppresses the cloud droplet growth and warm rain process under low static stability; nevertheless, the warm rain process is prevented regardless of aerosol concentration under a high static stability where a strong temperature inversion exists. Of course, the amount of the warm rain is minor compared with the cold-rain

process; thus the expected influence on the global hydrological cycle could be minimal in this case. Yet, this figure supports that the aerosols modulate the cloud life time through shutting off the warm rain formulation under the lower LTSS.

4. Uncertainties and Proposed Work

[17] Our study demonstrates an important sensitivity of the aerosol effect on the cloud-precipitation process to the different static stability regimes through a simultaneous examination of the cloud-top and columnar droplet effective radius. While the magnitude of its effect of cloud-top values, derived in this study, reproduces the value reported in the previous studies, those of columnar values are greater than the previous studies, suggesting a possible underestimation of the aerosols indirect effect with using cloud-top droplet size (*Nakajima et al.*, 2001). Yet, the following five uncertainties need to be solved for a more quantitative assessment of the aerosol indirect effect on the Earth's radiation budgets and for a validation of a parameterization of aerosol-cloud interactions within climate models.

i) Initial droplet spectra broadening associated with giant CCNs was not examined in this study.

ii) Cloud lifetime effect can be inferred from the precipitation efficiency. Nevertheless, the exact cloud lifetime cannot be obtained from the satellite observations alone.

iii) We cannot separate the effect of aerosols on the background thermodynamics and corresponding nonlinear feedback to the clouds.

The above issues are related to the dynamics and nonlinearity of cloud-precipitation process, and can not be examined through the observations alone. Aerosols scatter and absorb the radiation so as to directly change the thermodynamic profile in the planetary boundary layer, the pattern of large-scale circulation, and eventually the static stability elsewhere on the globe. These uncertainties can be examined through a numerical experiment with a bin-spectra cloud resolving model (CRM) [*Tao, 2003*].

iv) The vertical distribution of the aerosol concentration is not derived from the satellite-derived aerosol products.

It may be possible to combine the aerosol dataset from MODIS and a global chemical transport model to distinguish the aerosols above the warm cloud. Such transport is simulated, for example, in the dust aerosols from the Gobi and Sahara desert [*Ginoux et al.*, 2001].

v) Although the chemical compositions of aerosols vary significantly in different regions, aerosols are treated as a single aerosol index in this study.

This study shows the initial result which starts from March 2000 and is extended for a three month period. The TRMM and MODIS raw dataset are available from March 2000 to the present time (January 2004). Multi-seasonal and multi-year datasets will provide a sufficient sampling number to derive a statistically significant relationship at the regional scale.

[18] The interaction of aerosols and the thermodynamic structure with respect to how cloud and precipitation processes are affected is a critical and incompletely understood aspect of the Earth's climate system. This paper presents an analysis of the current global patterning of these combined effects.

Acknowledgements. This work is funded from CEAS fellowship through a joint collaboration between CSU and NASA GSFC. VIRS (1B01) and TMI (1B11) data were provided by NASA GSFC DAAC. NCEP/NCARR reanalysis were provided by the NOAA Climate Diagnostics Center. Authors thank to Allen Chu at NASA/GSFC to provide the MODIS aerosol and angstrom coefficient data (Level 1). Authors also thank to T. Y. Nakajima at NASDA/EORC for providing the GTR 4.1 packages.

References

Albrecht, B. A., Aerosols, cloud microphysics, and fractional cloudiness, *Science, 245*, 1227-1230, 1989.

Bréon, F.-M., D. Tanré, and S. Generoso, Aerosol effect on cloud droplet size monitored from satellite, *Science, 295*, 834-838, 2002.

Charlson R. J., S. E. Schwartz, J. M. Hales, R. D. Cess, J. A. Coakley Jr., J. E. Hansen, and D. J. Hofmann, Climate forcing by anthropogenic aerosols, *Science, 255*, 423-430, 1992.

Feingold, G., W. L. Eberhard, D. E. Veron, and M. Previdi, First measurements of the Twomey indirect effect using ground-based remote sensors, *Geophys. Res. Lett.*. **30(6)**, doi:0.029/2003GL017967, 2003.

Ginoux, P., M. Chin, I. Tegen, J. Prospero, B. Holben, O. Dubovik, and S.-J. Lin, Sources and global distributions of dust aerosols simulated with the GOCART model, *J. Geophys. Res., 106,* 20,255-20,273, 2001.

Hartmann, D. L., M. E. Ockert-Bell, and M. L. Michelsen, The effect of cloud type on earth's energy balance: Global analysis. *J. Clim., 5,* 1281-1304, 1992.

Johnson, R. H., B. D. Miner, and P. E. Ciesielski, Circulations between mesoscale convective systems along a cold front. *Mon. Wea. Rev.*, **123**, 585-599, 1995.

Kalnay *et al.*, The NCEP/NCAR 40-year reanalysis project. *Bull. Amer. Meteor. Soc., 77*, 437-471, 1996.

Kaufman, Y. J., D. Tanré, and O. Boucher, A satellite view of aerosols in the climate system, *Nature, 419*, 215-223, 2002.

Klein, S. A., and D. L. Hartmann, The seasonal cycle of low stratiform clouds., *J. Clim., 6,* 1587-1606, 1993.

Masunaga, H., T. Y. Nakajima, T. Nakajima, M. Kachi, R. Oki, and S. Kuroda, 2002a: Physical properties of maritime low clouds as retrieved by combined use of Tropical Rainfall Measurement Mission Microwave Imager and Visible/Infrared Scanner: Algorithm, *J. Geophys. Res. 107(10)*, doi:10.1029/2001JD000743, 2002a.

Masunaga, H., T. Y. Nakajima, T. Nakajima, M. Kachi, K. Suzuki, Physical properties of maritime low clouds as retrieved by combined use of Tropical Rainfall Measurement Mission Microwave Imager and Visible/Infrared Scanner 2. Climatology of warm clouds and rain, *J. Geophys. Res. 107(19),* doi:10.1029/2001JD001269, 2002b.

Nakajima, T., A. Higurashi, K. Kawamoto, and J. E. Penner, A possible correlation between satellite-derived cloud and aerosol microphysical parameters, *Geophys. Res. Lett., 28*, 1171-1174, 2001.

Rosenfeld, D., and G. Feingold, 2003: Explanation of discrepancies among satellite observations of the aerosol indirect effect, *Geophys. Res. Lett. 30(14),* doi;10.029/2003GL017684, 2003.

Schumacher, C., and R. A. Houze Jr., The TRMM Precipitation Radar's View of Shallow, Isolated Rain. *J. Appl. Meteorol., 42*, 1519-1524, 2003.

Tanré, D., Y. J. Kaufman, M. Herman, and S. Mattoo, Remote sensing of aerosol properties over oceans using the MODIS/EOS spectral radiance. *J. Geophys. Res.*, *102*, 16,971-16,988, 1997.

Tao, W.-K., 2003: Goddard Cumulus Ensemble (GCE) Model: Application for understanding precipitation processes, AMS Meteorological Monographs

Twomey, S. A., M. Piepgrass, and T. L. Wolfe, An assessment of the impact of pollution on global cloud albedo, *Tellus, 36B*, 356-366, 1984.

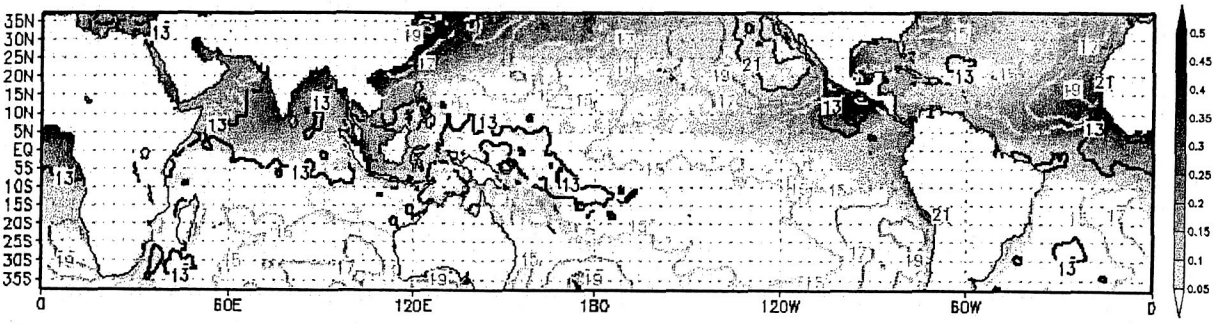

Figure 1. Global distribution of aerosol index (dark shaded) from the MODIS measurements and low-troposphere static stability LTSS (K) (colored contour) derived from the NCEP/NCAR reanalysis.

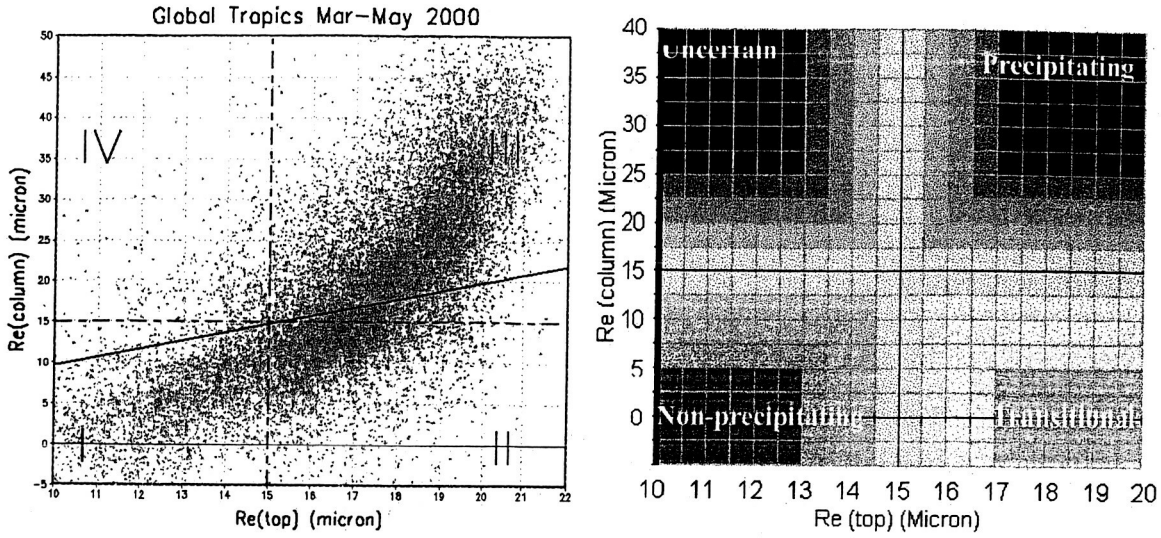

a b

Figure 2. a) Seasonally averaged Re (top) and Re (column) at each grid box are compared. Dash lines represent 15-micron drizzle threshold. Solid line shows the 1:1 ratio between Re (top) and Re (Column). b) Color coordination based on the warm cloud modes.

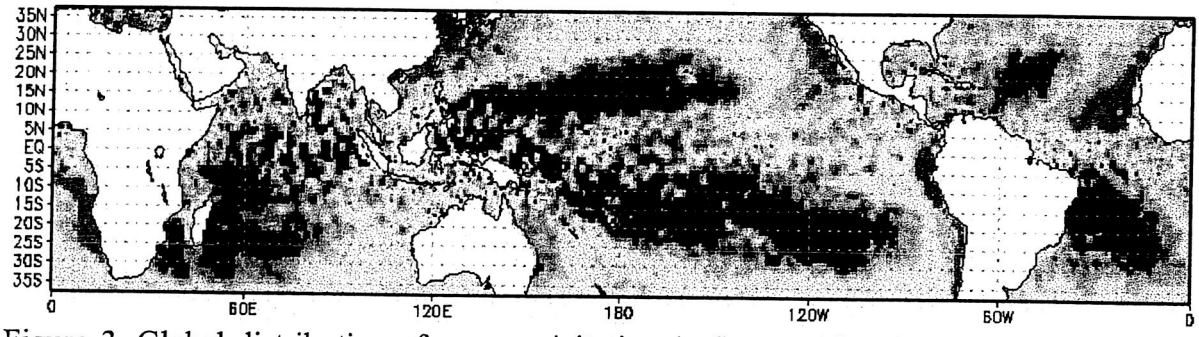

Figure 3. Global distribution of non-precipitating (red), transitional (green) and precipitating (blue) modes of warm cloud averaged through March-May in 2000. Color coordinates are based on Figure 1.b.

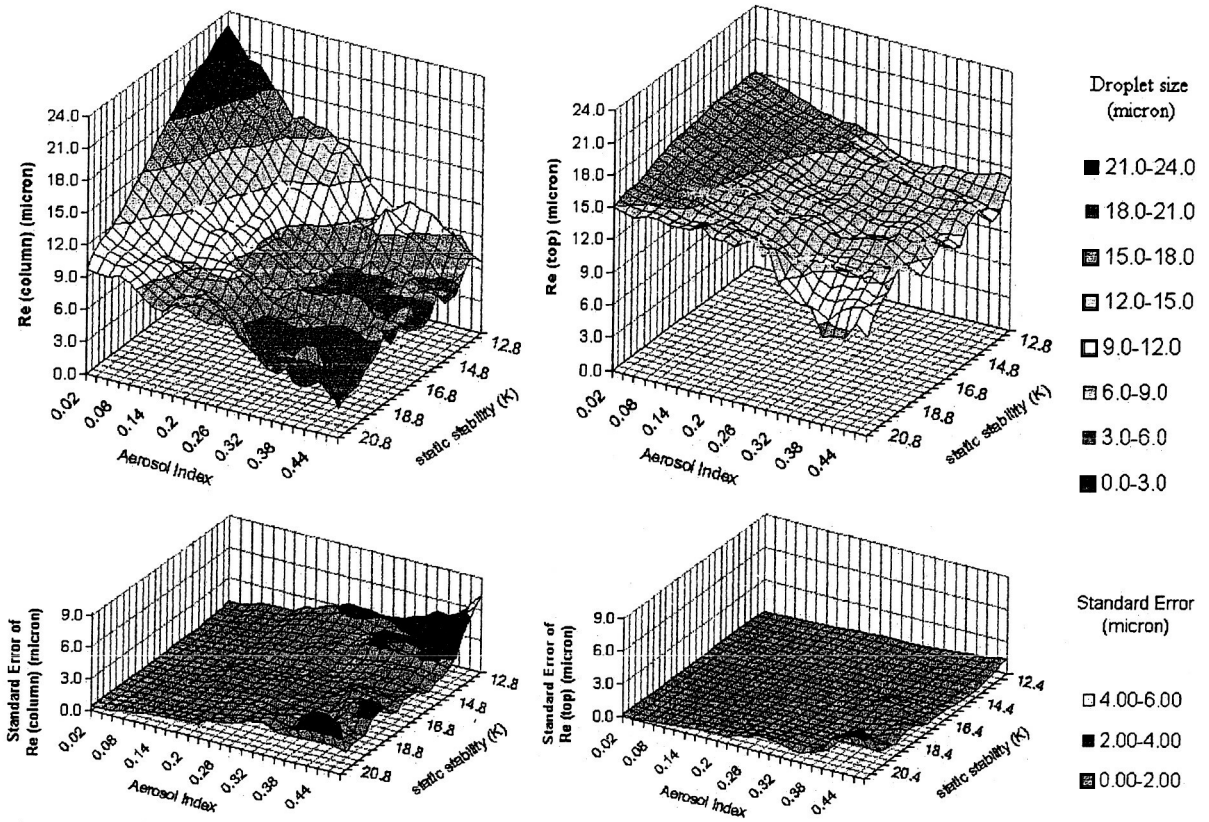

Figure 3. The mean and the standard error of Re (top) and Re (column) were derived for sets with a given aerosol index (bins of 0.01) and low-atmosphere static stability (bins of 0.4 K) on the global tropics from May to March.

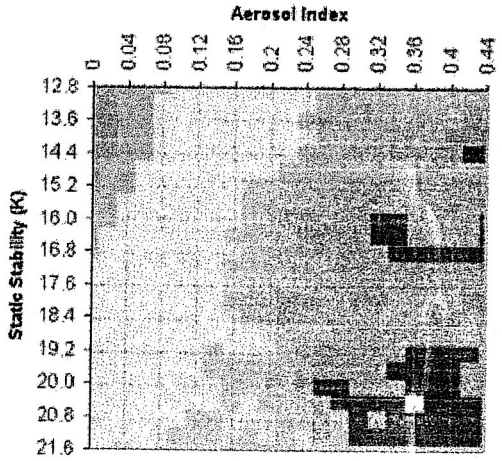

B

Figure 4. Re (column) and Re (top) are overlaid and colored based on the four types of warm cloud in Figure 1. B. Aerosol index and low-tropospheric static stability can determined the cloud modes.